

Effect of Physico-Chemical Interactions and Cyclic Wet-Dry Process on Behaviour of Compacted Clay Soils

T. Thyagaraj¹[0000-0002-5029-9472] and M. Julina²

¹Professor, Indian Institute of Technology Madras, Chennai – 600036, India

²Former Research Scholar, Indian Institute of Technology Madras, Chennai – 600036, India

Abstract. Physico-chemical interactions and alternate wetting and drying process have marked influence on the volume change and hydraulic behaviour of compacted clay soils used in geotechnical and geo-environmental engineering applications. The microstructure, desiccation cracks pattern and hydraulic behaviour of compacted clay soils get altered due to the physico-chemical interactions and cyclic wet-dry process. Therefore, the combined effect of concentration of interacting fluid and cyclic wet-dry process on the volume change, microstructure, desiccation cracks and hydraulic conductivity of compacted clay soil is studied in this paper. The desiccation cracks in compacted clays during a drying cycle was quantified using the X-ray computed tomography images and vernier caliper height measurement. And the same method was used to quantify the cracks in desiccated specimens interacted with different concentrations of interacting fluid. Scanning electron microscope and mercury intrusion porosimeter studies were carried out to understand the microstructure of salt solution interacted specimens. The influence of physico-chemical interactions and cyclic wet-dry process on the self-healing capacity of compacted clay specimens was brought out by carrying out hydraulic conductivity tests at the end of different wetting cycles.

Keywords: Desiccation Cracks, Hydraulic Conductivity, Interacting fluid, Microstructure.

1 Introduction

Compacted clays are considered as low hydraulic conductivity barriers ($k < 1 \times 10^{-7}$ cm/s) in various geotechnical and geo environmental applications including the landfill liners. In addition to its low hydraulic conductivity, the self-healing capacity of the clay against desiccation cracking decides the efficiency of the compacted clays as good barrier material. However, the exposure of these barriers to cyclic wet-dry process and physico-chemical interactions alter their volume change behaviour, hydraulic behaviour, and shrinkage and desiccation cracks pattern during drying.

In general, the compaction of soils results in the decrease of large pores between the soil particles. However, pores do exist in the compacted clay soils and the pores

are characterized with macrostructure and microstructure [1]. The macrostructure of compacted clays are not affected directly by physico-chemical interactions, whereas the microstructure of compacted clays changes due to physico-chemical interactions (from the contraction of diffused double layers), which results in altering the macro behaviour in particular the hydraulic conductivity of compacted clays [2-6]. Though the swell (volume change during wetting) and void ratio of compacted clays decrease with the increase in concentration of interacting fluid (IF), the hydraulic conductivity of these soils increased [2, 5-7]. Overall shrinkage and development of desiccation cracks occur during drying of compacted clays [2, 8, 9]. Due to the self-healing property of clay, these discontinuities in desiccated clay soils completely close during wetting, evidenced with low hydraulic conductivity when permeated with distilled water (DW) [5, 10, 11]. However, the macrostructural behaviour of compacted clays in terms of desiccation cracks pattern also gets altered due to physico-chemical interactions [2, 9, 12-14]. The visible cracks on the surface of clay specimens can be monitored using digital camera (DC) images, whereas, the interior cracks can only be visualized and quantified using advanced imaging experiments like X-ray computed tomography (XCT) experiments [2, 8, 9].

Previous research mainly focused on understanding the volume change and hydraulic behavioural changes of the compacted clay soils due to the effect of physico-chemical interactions, mainly from their as-compacted state. The experimental studies focusing on the combined effect of physico-chemical interactions and cyclic wet-dry process on the behaviour of compacted clay soils are limited and needs examination. Therefore, this paper details a method using XCT images and vernier caliper height measurement to quantify the desiccation cracks within the clay specimens. The combined effect of physico-chemical interactions in terms of concentration of IF and cyclic wet-dry process on the volume change, microstructure, desiccation cracks and hydraulic conductivity of compacted clay soil was also brought. The hydraulic conductivity of the compacted clay specimens interacted with different salt solutions at the end of first to fifth wetting cycles were related with their macropores size at the end of wetting cycles and cracks volume at the end of previous drying cycle.

2 Materials and Methods

For carrying out the oedometer cyclic wet-dry tests, the natural clay soil with properties tabulated in Table 1, was pulverized and sieved to pass through 2 mm sieve. Detailed methodology for preparation of compacted specimens (initial conditions: maximum dry density and optimum water content) and procedure for carrying out wet-dry cycles in the present study is described in Julina and Thyagaraj [2, 8] and Thyagaraj and Julina [5]. Identical compacted specimens with diameter of 7.54 cm and height of 2 cm were inundated with DW, 0.4M (Molar) sodium chloride (NaCl) and 4M NaCl solutions during different wetting cycles for understating the combined effect of physico-chemical interactions in terms of IF concentration and wet-dry cycles and the specimens are designated as DW, 0.4Na and 4Na specimens, respectively. During

drying cycles, all the specimens were allowed to dry till the water content of swollen specimens reduced to a water content around 4%. The height and diameter of the specimens at the end of wetting cycles, during and at the end of drying cycles were measured using vernier calipers. And during both wetting and drying process, 12.5 kPa vertical stress was maintained on the top of the specimens. "ImageJ" software [15] was used to carry out binary imaging technique on XCT images for the quantification of desiccation cracks. The microstructure of the compacted specimens at the as-compacted state (initial condition) and at the end of different wetting cycles were studied using scanning electron microscope (SEM) images and pore size density functions (PSD's) obtained from mercury intrusion porosimeter studies. And the hydraulic conductivity of the completely swollen specimens (i.e. at the end of different wetting cycles) were determined using oedometer rigid wall permeameters.

Table 1. Properties of the natural clay soil [3-5, 13].

Soil property	Value
Grain size distribution	
Sand (%)	3
Silt (%)	15
Clay (%)	82
Atterberg limits	
Liquid limit (%)	78
Plastic limit (%)	27
Shrinkage limit (%)	9
Unified soil classification symbol	CH
Free swell index (%)	105
Specific gravity	2.71
Cation exchange capacity (meq/100g)	58.71
Standard Proctor compaction characteristics	
Maximum dry density (MDD, Mg/m ³)	1.34
Optimum moisture content (OMC, %)	28

3 Quantification of Desiccation Cracks

Fig. 1 presents the volumetric deformation of DW specimen calculated using vernier caliper average height and diameter measurements and Eq. 1 [2] at the end of five wet-dry cycles.

$$\text{Volumetric deformations (\%)} = \frac{V_{total} - V_{com}}{V_{com}} \times 100 \quad (1)$$

Where V_{total} is the overall volume of the compacted specimens including cracks volume (V_{cracks}) at the end of either wetting or drying cycles and V_{com} is the volume of as-compacted specimen.

Volume increase occurs in the vertical direction during the first wetting cycle and, in both vertical and lateral directions during the second and consequent wetting cycles owing to the swelling of clay particles upon absorption of water in DW specimen.

During drying cycles, water loss owing to evaporation leads to the reduction of the volume of DW specimen. In addition to vertical settlement, discontinuities develops in the form of desiccation cracks within the shrunken specimen and the annular gap between the shrunken specimen and oedometer ring during drying cycles in compacted clay specimens (indicated in Fig. 2). These discontinuities hinder the determination of correct volume of desiccated specimens using vernier caliper measurements. Advanced imaging experiments using XCT assists in capturing the interior of desiccated specimens. Julina and Thyagaraj [2, 8, 9] utilized the XCT horizontal sectional images (50 slices from top surface to bottom surface), binary image processing technique and vernier caliper height measurements to determine the cracks volume in desiccated specimens. The cracks volume was used to calculate the volumetric deformations, pore void ratio and other void ratios accurately [2, 8].

Specimen designation	Deformations measured using vernier		Shrinkage deformations measured using XCT and vernier	Deformations			
	Swell	Shrink		Total volumetric		Shrinkage	
				Vernier	XCT and vernier	Vernier	XCT and vernier
DW				38.3	43.3	21	26
0.4Na				39.1	44	23	27.9
4Na				10.5	26.3	0.7	15.8

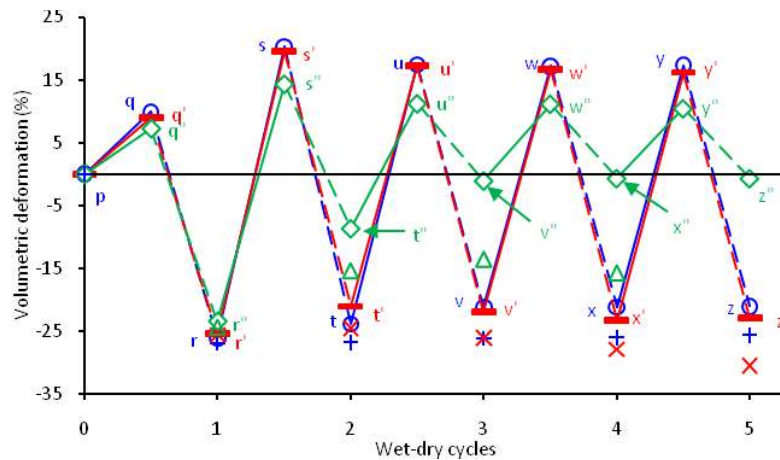
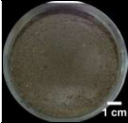
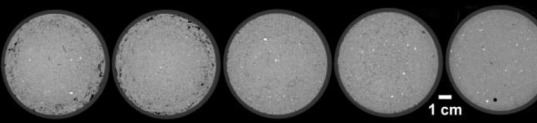
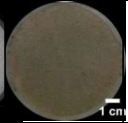
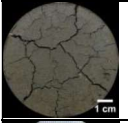
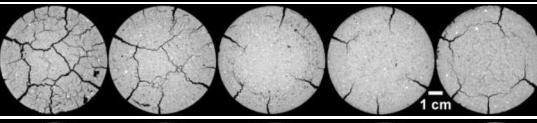
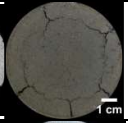
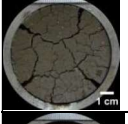
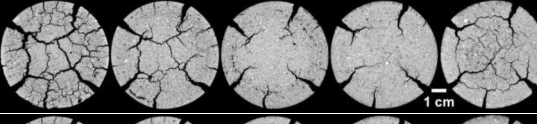
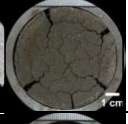
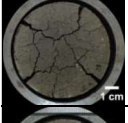
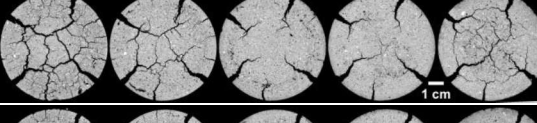
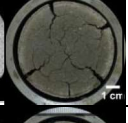
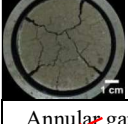
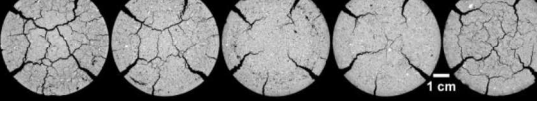
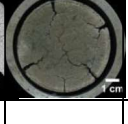
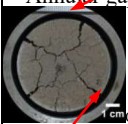
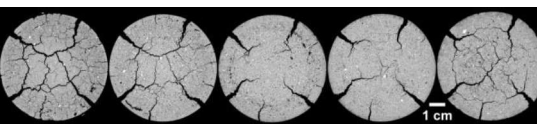
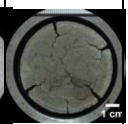


Fig. 1. Comparison of volumetric deformations of DW, 0.4Na and 4Na specimens using vernier caliper measurement at the end of each wet-dry cycles and XCT images and height measured using vernier caliper at the end of different drying cycles [2, 5]

Fig. 2 shows the surface DC and horizontal sectional XCT (five images corresponding to 2, 20, 48, 70 and 98% depths) images of DW specimen during the second drying cycle. Fig. 3 presents the variation of cracks area (A_{cracks}) with depth of DW specimen during the second drying cycle and also compares the variation of cracks area at different water contents. At the beginning of the second drying cycle (i.e. at the end of the second wetting cycle) the completely swollen DW specimen is devoid of annular gap and desiccation cracks (images pertaining to water content of 52.4% are shown in Fig. 2).

Top surface DC images	XCT images at 2, 20, 48, 70 and 98% depth of specimen	Bottom surface DC images	w (%)
			*52.4
			38.5
			28.3
			16.5
			10.3
			4.02

* - identical soil specimen; bottom surface DC images should be viewed in opposite direction

Fig. 2. Surface DC and horizontal interior sectional XCT images of DW specimen during second drying cycle [8]

During drying, the desiccation cracks within the shrunken specimen develop in two distinct forms, namely, propagating (wider cracks in the edges which radially reduced towards the center and propagates through the entire thickness of the desiccated specimen) and non-propagating cracks (cracks present only near the top and bottom sur-

faces) (Fig. 2). At all the water contents during drying, the cracks area decreases gradually from the top surface towards the mid-depth of the specimen and then increases gradually towards the bottom surface of the specimen (Fig. 3). The comparatively higher cracks area at the top and bottom surfaces in the desiccated specimen is attributed to the presence of non-propagating cracks in addition to the propagating cracks (Figs. 2 and 3). The cracks area of desiccated specimen during drying was found to increase above the mid-depth at all water contents due to the presence of a horizontal crack (Fig. 3). The desiccated specimens tend to undergo global shrinkage during drying and hence the cracks area increased till 28.3% beyond which it decreased (Figs. 2 and 3). The decrease in cracks area of the desiccated specimen ceased when the water content reached near the shrinkage limit water content.

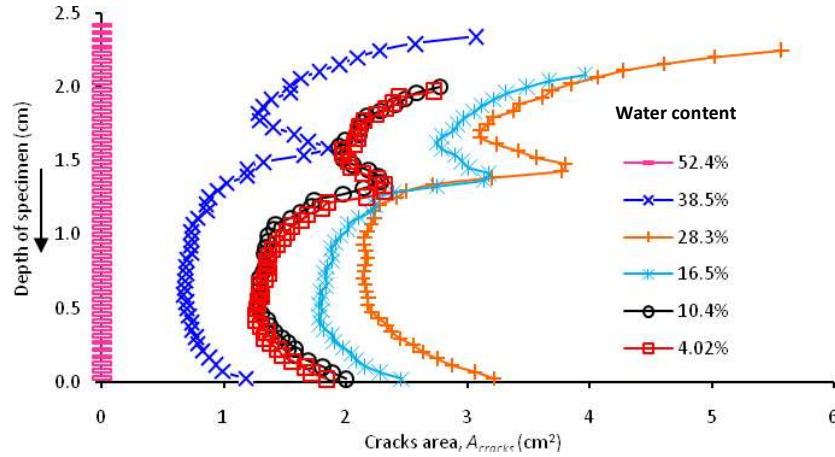


Fig. 3. Variation of cracks area with depth of DW specimen during second drying cycle [8]

The cracks volume within the desiccated specimens during and at the end of drying process is calculated using Eq. 2 [2, 8]. Fig. 1 also presents the volumetric deformation at the end of drying cycles of DW specimen calculated using XCT images and vernier caliper height measurement, and Eqs. 2 and 3 [2].

$$V_{cracks} = \text{Average } A_{cracks} \text{ of 50 horizontal slices} \times \text{height of specimen (cm}^3) \quad (2)$$

$$\text{Volumetric deformations (\%)} = \frac{V_{total} - V_{cracks} - V_{com}}{V_{com}} \times 100 \quad (3)$$

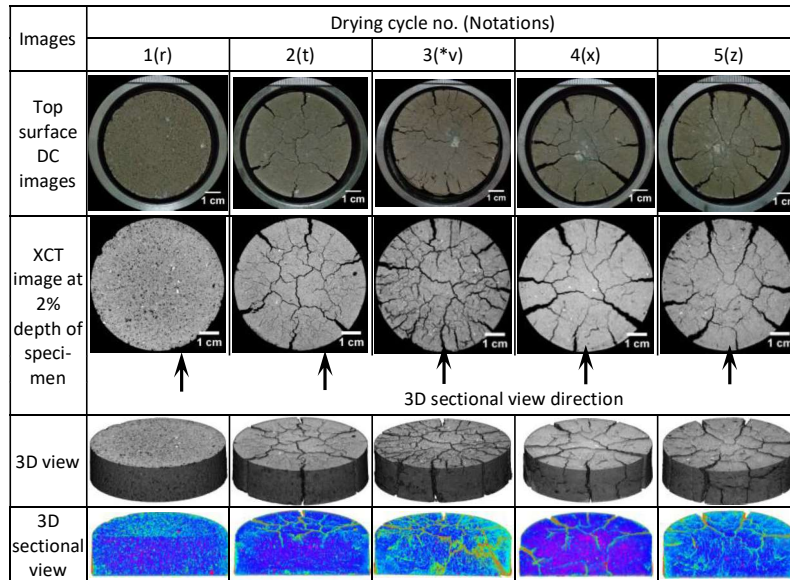
As the cracks volume is excluded using XCT images and vernier caliper height measurement method, 5% increase in both shrinkage and total volumetric deformations of DW specimen was observed at the equilibrium wet-dry cycles in comparison to shrinkage and total volumetric deformations calculated using vernier caliper measurements (Fig. 1).

4 Effect of Physico-Chemical Interaction And Cyclic Wet-Dry Process

Fig. 1 also brings out the effect of physico-chemical interaction and cyclic wet-dry process on volumetric deformation of DW, 0.4Na and 4Na specimens calculated using vernier caliper measurements, and XCT images and vernier caliper height measurement. The high concentration of salt in IF than the pore fluid within the 0.4Na and 4Na specimens caused the osmotic-induced consolidation and osmotic consolidation during wetting. Hence for both the measurement methods, the magnitude of volumetric deformations of compacted specimens decreased with the increase in IF concentration during all the cycles (Fig. 1).

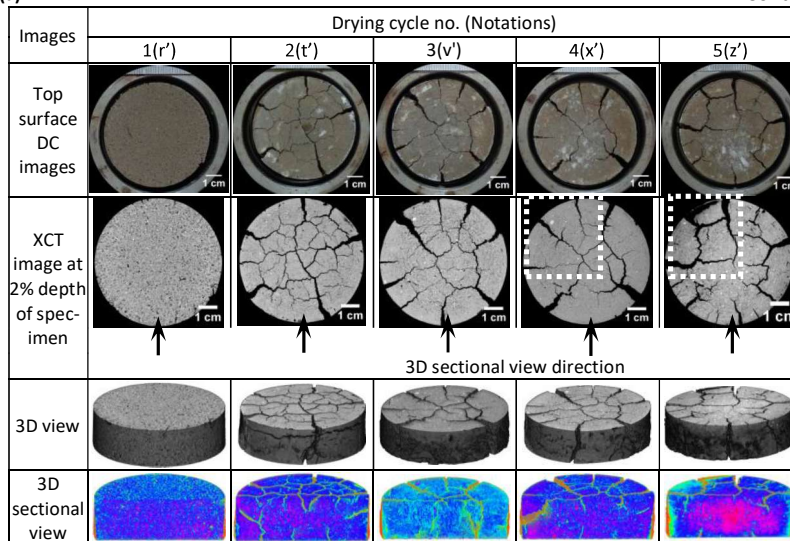
4.1 Desiccation Cracks

Figs. 4(a), (b) and (c) show the surface DC, near surface horizontal sectional XCT, and reconstructed 3D and 3D sectional XCT images at the end of first to fifth drying cycles of DW, 0.4Na and 4Na specimens, respectively. The desiccation cracks pattern at the end of each drying cycles of DW, 0.4Na and 4Na specimens differed due to physico-chemical interactions and cyclic wet-dry process. In all the desiccated specimens, propagating and non-propagating cracks were developed at the end of second to fifth drying cycles (Fig. 4). For DW and 0.4Na specimens, the development of cracks stabilized at the equilibrium wet-dry cycles and hence the volumetric deformation attained a constant value (Figs. 1, 4(a) and 4(b)). The self-healing capacity of desiccated DW specimen assisted in complete closure of discontinuities during wetting which is evident from the development of cracks at different positions within the desiccated DW specimen at the end of second to fifth drying cycles (Fig. 4(a)). As the salt concentration within the 0.4Na specimen gradually increases with the increase in number of wet-dry cycles, the self-healing capacity of this 0.4Na specimen was found to reduce after four wet-dry cycles, evidenced by the presence of few propagating cracks at same positions, indicated in Fig. 4(b). Though cracks on the surface of 4Na specimen are not visible in DC images, XCT images showed that the interior of the specimen was porous and the cracks were present at the same position at the end of second to fourth drying cycles (Fig. 4(c)). This behaviour of 4Na specimen indicates that the self-healing capacity of the compacted clay soils gets completely destroyed due to interaction with higher concentration salt solutions during wet-dry cycles.

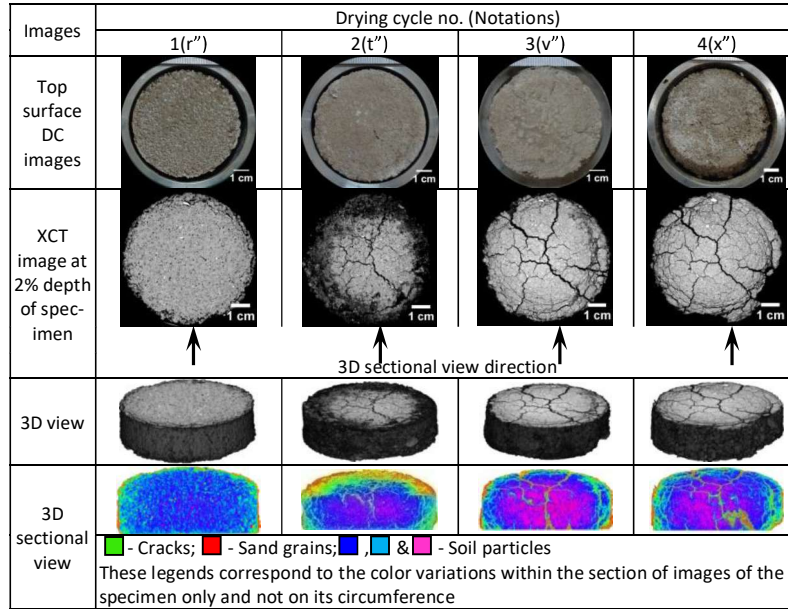


*-identical soil specimen

(a) Cont.,



(b)



*: the difference in color among the DC images of 4Na specimen is due to the salt precipitation

(c)

Fig. 4. Top surface DC images, near surface horizontal sectional XCT images, and 3D and 3D sectional XCT images (not to scale) at the end of different drying cycles of: (a) DW, (b) 0.4Na and (c) 4Na specimens (as per the notations labeled in Fig. 1) [2]

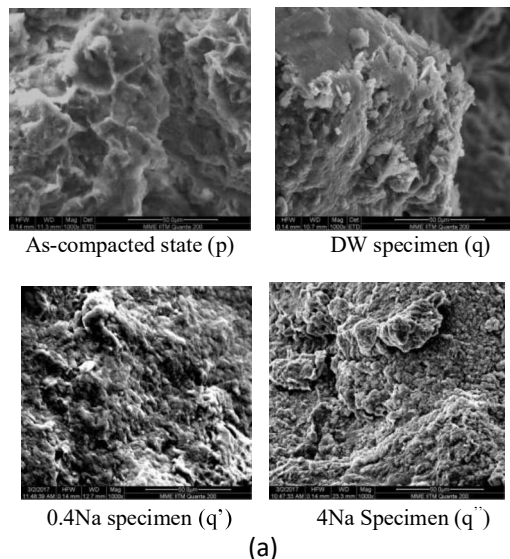
4.2 Microstructure

Fig. 5(a) shows the SEM images of DW, 0.4Na and 4Na specimens at the initial as-compacted state and swollen state at the end of first wetting cycle. Figs. 5(b), (c) and (d) compare the PSDs of DW, 0.4Na and 4Na specimens at the initial as-compacted state and swollen state at the end of the first, second and fifth wetting cycles, respectively. The SEM images and PSDs of DW, 0.4Na and 4Na specimens displayed bimodal structure at the as-compacted state (macropores peak size: around 64 μm) and swollen state at the end of first wetting cycle (Figs. 5(a) and (b)). The macropores peak shifted leftward from the as-compacted state for DW, 0.4Na and 4Na specimens at the end of first wetting cycle owing to the evolution of micropores and eventual reduction of macropores during swelling (Fig. 5(b)). However, at the end of first wetting cycle the interaction of higher concentration of salt solution (4M NaCl solution) during wetting of 4Na specimen resulted in marginal leftward shift (around 61 μm) of the macropores peak from as-compacted state than swollen DW and 0.4Na specimens. This behaviour is attributed to the reduction in the micropores volume from osmotic consolidation and osmotic-induced consolidation which occurs due to the increase in the concentration of IF. Interaction of 4M NaCl solution during subsequent wetting cycles resulted in marked increase in macropores size and volume within the

range of 10 and 135 μm in 4Na specimen than DW and 0.4Na specimens (Figs. 5(c) and (d)).

4.3 Hydraulic Conductivity

Fig. 6 brings out the effect of physico-chemical interactions and cyclic wet-dry process on the hydraulic conductivity of DW, 0.4Na and 4Na specimens. The hydraulic conductivity determined at the end of first to fifth wetting cycles of 0.4Na and 4Na specimens increased with the increase in the IF concentration. As the complete closure of discontinuities occurs during wetting of desiccated DW specimens, the hydraulic conductivity of DW specimen did not increase significantly at the end of first to fifth wetting cycles. Whereas, the hydraulic conductivity of 0.4Na and 4Na specimens increased marginally and significantly, respectively, with the increase in the number of wet-dry cycles (Figs. 5 and 6). In particular, two order increase in hydraulic conductivity was observed at the equilibrium wet-dry cycles of 4Na specimen than DW specimen (Fig. 6). This hydraulic behaviour is due to larger macropores size and volume (range: 10 to 135 μm) of swollen 4Na specimen at the end of wetting cycles (Fig. 5). Fig. 7 relates the cracks and annular gap volumes of DW, 0.4Na and 4Na specimens at the end of different drying cycles with the hydraulic conductivity of the specimens at the end of subsequent wetting cycles. The cracks and annular gap volumes was significantly higher and lower, respectively, for the 4Na specimen in comparison to DW and 0.4Na specimens at the end of second to fifth drying cycles (Fig. 7). Even though the annular gap volume and the volumetric deformation of desiccated 4Na specimen was less than desiccated DW and 0.4Na specimens, the hydraulic conductivity of 4Na specimen increased significantly after second wetting cycle (Figs. 1, 6 and 7). It is evident from the hydraulic conductivity and microstructural studies that



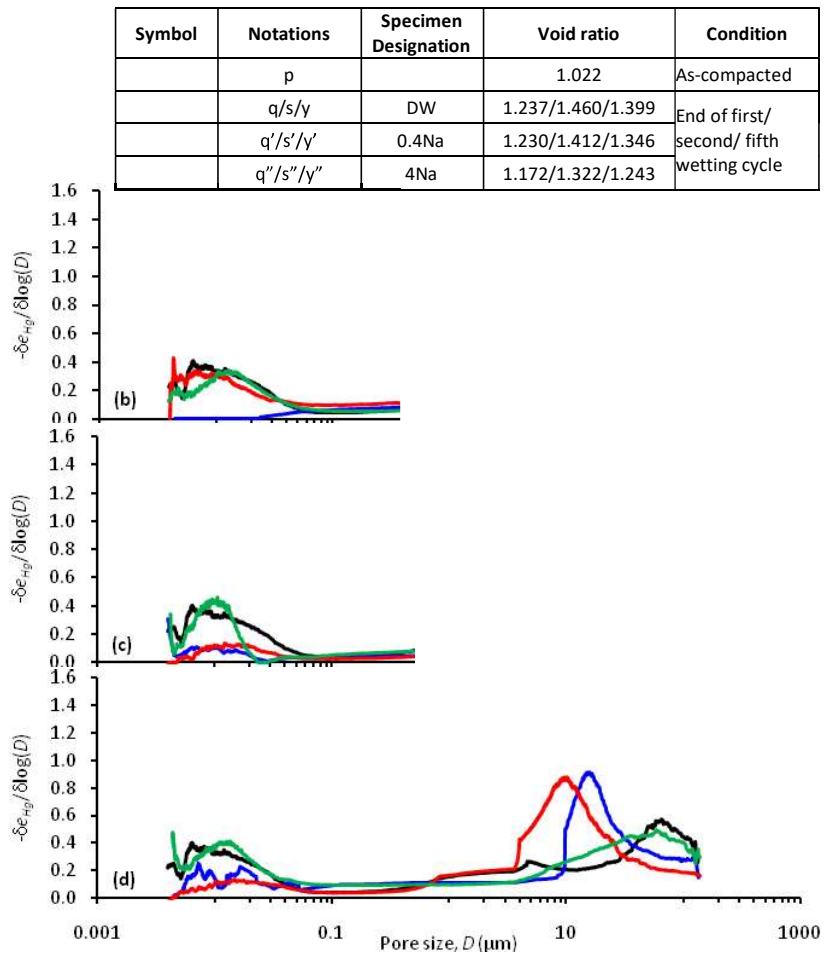


Fig. 5. (a) SEM images of DW, 0.4Na and 4Na specimens at the initial as-compacted state and swollen state at the end of first wetting cycle; and comparison of PSD plots of DW, 0.4Na and 4Na specimens at the as-compacted state and swollen state at the end of: (b) first, (c) second and (d) fifth wetting cycles (as per the notations labeled in Fig. 1) [5]

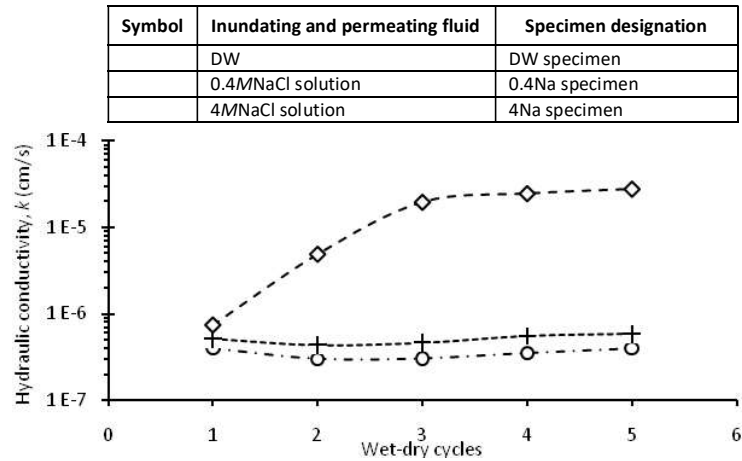


Fig. 6. Effect of physico-chemical interactions and cyclic wet-dry process on the hydraulic conductivity of DW, 0.4Na and 4Na specimens [5]

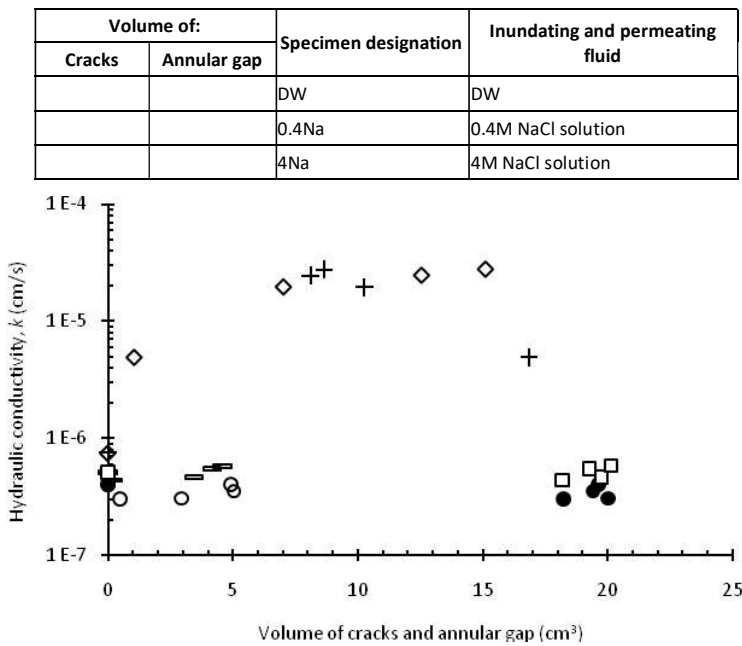


Fig. 7. Relation between hydraulic conductivity of DW, 0.4Na and 4Na specimens at the end of wetting cycles and volume of cracks and annular gap of DW, 0.4Na and 4Na specimens at the end of previous drying cycles [2]

the exposure of compacted clay soils to higher concentration of salt solution and wet-dry cycles result in complete loss of self-healing capacity of clay particles.

5 Summary and Conclusions

This paper briefly describes a method using XCT images and vernier caliper height measurement to accurately quantify the cracks volume of desiccated specimens. The same method was used to study the cracks pattern of DW and salt solution interacted specimens during and at the end of different drying cycles. And the influence of physico-chemical interactions and cyclic wet-dry process on the volume change behaviour, microstructure and hydraulic conductivity of compacted clay soils was also studied.

Upon interaction of clays with higher concentration salt solution (4Na specimen), the evolution of microstructure during swelling reduces due to osmotic-induced consolidation and osmotic consolidation and hence the macropores size and volume of this specimen were significantly higher than the DW specimen at the end of first wetting cycle. Repetitive exposure of 4Na specimen to wetting and drying process not only result in the further increase of macropores size and volume but also resulted in the development of desiccation cracks at the same position after the second drying process. In addition, the porous microstructure of 4Na specimen resulted in considerable increase in hydraulic conductivity, mainly after the second wetting cycle. On the other hand, only marginal increase in hydraulic conductivity was observed in 0.4Na specimen (clay specimen interacted with lower concentration salt solution) than the DW specimen even after the second wetting cycle. However, the development of few cracks at the same positions after the fourth drying process suggest that the 0.4Na specimen may also become more porous when subjected to more number of cyclic wet-dry process. Hence, based on this experimental study, it can be concluded that the self-healing property of clay soils gets considerably reduced due to its exposure to physico-chemical interactions and cyclic wet-dry process.

References

1. Gens, A., Alonso, E.E.: A framework for the behavior of unsaturated expansive clays. *Canadian Geotechnical Journal* 29(6), 1013-1032(1992).
2. Julina, M., Thyagaraj, T.: Combined effect of wet-dry cycles and interacting fluid on desiccation cracks and hydraulic conductivity of compacted clay. *Engineering Geology* 267, 1–15 (2020).
3. Mesri, G., Olson, R.E.: Mechanisms controlling the permeability of clays. *Clays and Clay Minerals* 19, 151–158 (1971).
4. Musso, G., Romero, E., Vecchia, G.D.: Double-structure effects on the chemo-hydro-mechanical behaviour of a compacted active clay. *Géotechnique* 63(3), 206–220 (2013).
5. Thyagaraj, T., Julina, M.: Effect of pore fluid and wet-dry cycles on structure and hydraulic conductivity of clay. *Geotechnique Letters* 9(4), 348-354 (2019).

T. Thyagaraj and M. Julina

6. Thyagaraj, T., Thomas, S.R., Das, A.P.: Physico-chemical effects on shrinkage behavior of compacted expansive clay. *International Journal of Geomechanics*, 17(2), 06016013, 1-11 (2016).
7. Rao, S.M., Thyagaraj, T., Thomas, H.R.: Swelling of compacted clay under osmotic gradients. *Géotechnique*, 56(10), 707–713(2006).
8. Julina, M., Thyagaraj, T.: Quantification of desiccation cracks using X-ray tomography for tracing shrinkage path of compacted expansive soil. *Acta Geotechnica* 14, 35-56 (2019).
9. Julina, M., Thyagaraj, T.: Application of X-ray computed tomography for capturing the desiccation cracks of soils. In: 7th Indian Young Geotechnical Engineers Conference – 7IYGEC 2019, pp. 428-433, NIT Silchar, Assam, India, March, 15-16 (2019).
10. Lin, L.C., Benson, C.H. : Effect of wet-dry cycling on swelling and hydraulic conductivity of GCLs. *Journal of Geotechnical and Geoenvironmental Engineering* 126 (1), 40–49 (2000).
11. Tay, Y.Y., Stewart, D.I., Cousens, T.W.: Shrinkage and desiccation cracking in bentonite-sand landfill liners. *Engineering Geology*, 60 (1–4), 263–274 (2001).
12. Gebrenegus, T., Ghezzehei, T.A., Tuller, M.: Physicochemical controls on initiation and evolution of desiccation cracks in sand–bentonite mixtures: X-ray CT imaging and stochastic modeling. *Journal of Contaminant Hydrology* 126, 100–112 (2011).
13. Shin, H., Santamarina, J.C.: Desiccation cracks in saturated fine-grained soils: particle-level phenomena and effective-stress analysis. *Géotechnique* 61 (11), 961–972 (2011).
14. Zhang, Y., Ye, W., Chen, B., Chen, Y.G., Ye, B.: Desiccation of NaCl-contaminated soil of earthen heritages in the Site of Yar City. northwest China. *Applied Clay Science*, 124-125, 1–10 (2016).
15. Rasband, W.S., *ImageJ*. Bethesda, MD: National Institutes of Health. <https://imagej.nih.gov/ij/>, 1997–2016 (2006).